Technical Sciences
Academy of Romania
www.jesi.astr.ro

Journal of Engineering Sciences and Innovation
Volume 6, Issue 2 / 2021, pp. 91-106

A. Mechanical Engineering

Received ***10 December 2020*** *Accepted* ***17 May 2021***
Received in revised from ***10 February 2021***

Modal analysis of a circular disc using the QLP decomposition of FRF matrices

MIRCEA RADEŞ*

Strength of Materials Department, Politehnica University of Bucharest,
Splaiul Independenţei 313, Bucharest, Romania

Abstract. A circular disc is used to demonstrate the application of the pivoted QLP decomposition to the analysis of the frequency response data for a structure possessing double modes. Frequency Response Functions (FRFs) are generated for excitation and response points on the disc rim. Plots of *L*-values and *Q*-response functions obtained by the QLP decomposition with column pivoting are used to determine the system order, damped natural frequencies and modal damping ratios, as well as mode shapes. The performance of the LMIF, QMIF and QCoMIF mode indicator functions is assessed in the presence of degenerate modes. Enhanced FRFs based on QRFs are used with single degree of freedom parameter identification techniques.

Keywords: pivoted QLP decomposition, circular disc, LMIF, QMIF, QCoMIF, QeFRF.

1. Introduction

Circular plates and discs have natural modes of transverse vibration defined by nodal diameters and nodal circles. Modes with only nodal circles are singular while those with nodal diameters occur in pairs of orthogonal double modes with identical natural frequencies. In a modal survey it is important to detect the existence of double modes, to identify their characteristics and include their contribution in the construction of a mathematical model. This paper illustrates the performance of the new mode indicators LMIF, QMIF and QCoMIF and the QeFRFs in the modal analysis of a free-free stationary perfectly symmetric circular disc.

*Correspondence address: rades@accessmedia.ro

2. FE model of the circular disc

We consider a freely supported circular disc vibrating in a direction normal to its plane. The FE model of the disc (Fig.1) was built with a mesh consisting of 12 equidistant diameters and 8 equidistant circles. The model contains 193 nodal points, each having three degrees of freedom, two rotations and a linear displacement. The mass and stiffness matrices are of the order 579. In order to generate realistic FRFs, 1 percent modal damping was added to the model, resulting in a non-proportionally lightly damped structure.
The simulated FRFs used in the analysis are receptances restricted to the 24 "edge" nodes lying on the rim of the disc, considering only transverse displacements and normal excitation forces. This way, the reduced normal modes have only 24 elements. The selected "excitation" points are a subset of the response "measurement" points.

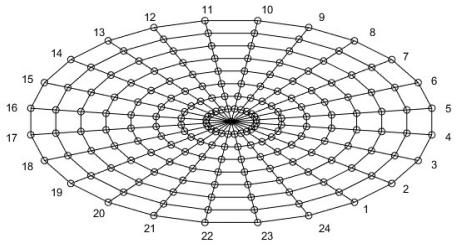

Fig. 1. Circular disc.

3. Natural frequencies and mode shapes

The lowest 12 undamped natural frequencies are presented in Table 1. The first three values corresponding to the rigid body modes are not included. In the frequency range 200 to 1800 Hz the disc has 12 flexible modes, two single modes and 5 pairs of double modes. Modes are conveniently labelled "*s/n*", where *s* is the number of nodal circles and *n* is the number of nodal diameters.

Table 1. Undamped natural frequencies

Mode nr.	Undamped natural frequency, Hz	*s/n*	Mode nr.	Undamped natural frequency, Hz	*s/n*
4	334.21	0/2	10	932.698	1/1
5	334.21	0/2	11	1252.37	0/4
6	408.69	1/0	12	1252.37	0/4
7	721.33	0/3	13	1605.72	2/0
8	721.33	0/3	14	1644.36	1/2
9	932.698	1/1	15	1644.36	1/2

The shapes of the first 12 flexible modes are shown in Fig.2 as instantaneous maximum values of the travelling modes. The damped natural frequencies and the imaginary part of the reduced mode shapes, with elements pertaining to the

transverse displacements of the edge nodes, are given in Table 2. Node 1 has been chosen as the reference node. This corresponds to the case when a force is applied at node 1. When the force is applied at node 2, the mode shapes are shifted.
The reduced modal vector corresponding to the first of each pair of frequencies is a symmetric "*cos*" mode of equation

$$x = \cos\ (j-1)\frac{2\pi n}{N}, \qquad (1)$$

where N =24, n is the number of nodal diameters and j is the station index $(j = 1,..,24)$.

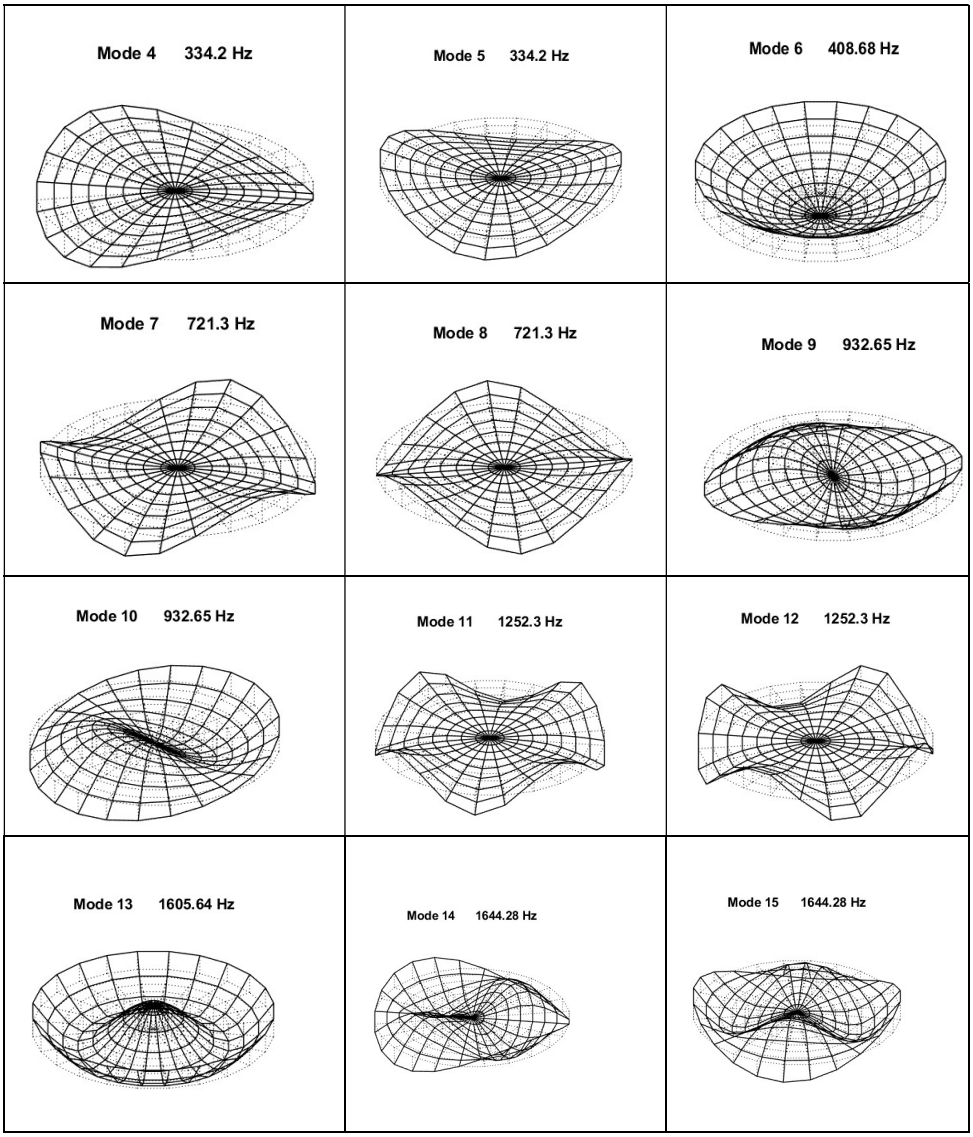

Fig. 2. Mode shapes of the axisymmetric disc.

Table 2. Damped natural frequencies and mode shapes of axisymmetric disc

	Mode shape											
	4	5	6	7	8	9	10	11	12	13	14	15
Node nr.0	Natural frequencies, Hz											
	334.2		408.7	721.3		932.65		1252.3		1605.6	1644.3	
	Displacement amplitude											
1	1	0	1	1	0	1	0	1	0	1	1	0
2	0.866	0.5	1	0.707	0.707	0.966	0.259	0.5	0.866	1	0.866	0.5
3	0.5	0.866	1	0	1	0.866	0.5	-0.5	0.866	1	0.5	0.866
4	0	1	1	-0.707	0.707	0.707	0.707	-1	0	1	0	1
5	-0.5	0.866	1	-1	0	0.5	0.866	-0.5	-0.866	1	-0.5	0.866
6	-0.866	0.5	1	-0.707	-0.707	0.259	0.966	0.5	-0.866	1	-0.866	0.5
7	-1	0	1	0	-1	0	1	1	0	1	-1	0
8	-0.866	-0.5	1	0.707	-0.707	-0.259	0.966	0.5	0.866	1	-0.866	-0.5
9	-0.5	-0.866	1	1	0	-0.5	0.866	-0.5	0.866	1	-0.5	-0.866
10	0	-1	1	0.707	0.707	-0.707	0.707	-1	0	1	0	-1
11	0.5	-0.866	1	0	1	-0.866	0.5	-0.5	-0.866	1	0.5	-0.866
12	0.866	-0.5	1	-0.707	0.707	-0.966	0.259	0.5	-0.866	1	0.866	-0.5
13	1	0	1	-1	0	-1	0	1	0	1	1	0
14	0.866	0.5	1	-0.707	-0.707	-0.966	-0.259	0.5	0.866	1	0.866	0.5
15	0.5	0.866	1	0	-1	-0.866	-0.5	-0.5	0.866	1	0.5	0.866
16	0	1	1	0.707	-0.707	-0.707	-0.707	-1	0	1	0	1
17	-0.5	0.866	1	1	0	-0.5	-0.866	-0.5	-0.866	1	-0.5	0.866
18	-0.866	0.5	1	0.707	0.707	-0.259	-0.966	0.5	-0.866	1	-0.866	0.5
19	-1	0	1	0	1	0	-1	1	0	1	-1	0
20	-0.866	-0.5	1	-0.707	0.707	0.259	-0.966	0.5	0.866	1	-0.866	-0.5
21	-0.5	-0.866	1	-1	0	0.5	-0.866	-0.5	0.866	1	-0.5	-0.866
22	0	-1	1	-0.707	-0.707	0.707	-0.707	-1	0	1	0	-1
23	0.5	-0.866	1	0	-1	0.866	-0.5	-0.5	-0.866	1	0.5	-0.866
24	0.866	-0.5	1	0.707	-0.7070	0.966	-0.259	0.5	-0.866	1	0.866	-0.5

The reduced modal vector corresponding to the second of each pair of frequencies is an antisymmetric "*sine*" mode of equation

$$y = \sin\,(j-1)\frac{2\pi n}{N}, \qquad (2)$$

rotated by an angle $\pi/2n$ with respect to the first.

Mode 6 is an "umbrella" mode in which all edge stations have uniform displacements. Mode 13 is a two nodal circle mode. If the mesh has insufficient radial resolution (only a few circles), this mode is not described by the FE model.

The reduced modal vectors are orthogonal, e.g. $\{u\}_r^T\,\{u\}_q = 0$, and are normalized with the largest element equal to unity. $\frac{1}{\sqrt{12}}\{u\}_r^T\,\frac{1}{\sqrt{12}}\,\{u\}_r = 1$.

For a perfectly symmetric disc there is no preferred orientation of the mode with respect to the free-free disc. Due to the axial symmetry it is possible to rotate the mode shape through any angle without changing the frequency of vibration. Any linear combination of the two orthogonal modal vectors in a pair is also an eigenvector. In complex notation, the two orthogonal mode shapes in a pair represent a *rotating normal mode*, described by standing waves defined by given values of the propagation constant [1].When the disc is acted upon by a harmonic force, the mode orients itself such that the point of maximum deflection is aligned with the excitation force [2].

When the symmetry is imperfect (mistuned disc), the two modes have different close natural frequencies, the nodal lines are fixed in the disc and not moving around to follow the excitation. Such *fixed modes*, determined using a very small detuning mass, are useful in the calculation of FRFs by mode summation. In a mass-mistuned disc, for each pair of modes the "*sine*" mode remains unchanged with a higher frequency while the "*cos*" mode has a lower natural frequency.

4. Plots of Frequency Response Functions

A system with non-proportional damping has complex valued FRFs. At each frequency ω the FRF matrix can be computed either by mode summation or as the inverse of the system matrix $[K] - \omega^2[M] + i\omega[C]$.

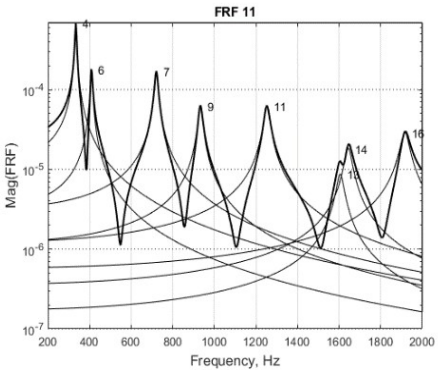

Fig.3. Plot of FRF11.

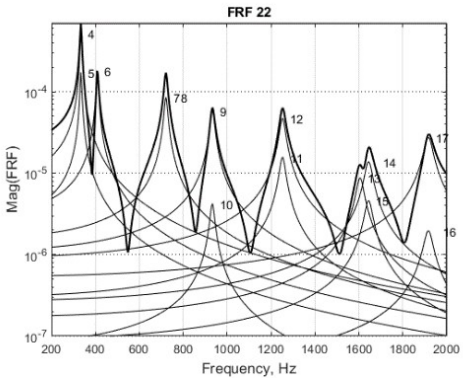

Fig.4. Plot of FRF22.

The FRF plots used in the simulation study are shown as magnitude (log scale) versus frequency (linear scale) plots. Receptance frequency response functions $FRFjk = H_{jk}(\omega)$ have been simulated for displacement at point j due to the excitation at point k. Overlaid curves of the contributing fixed modes of vibration correspond to the respective term in the partial fraction format.

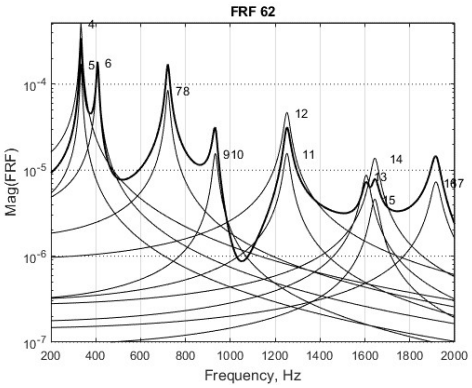

Fig. 5. Plot of FRF62.

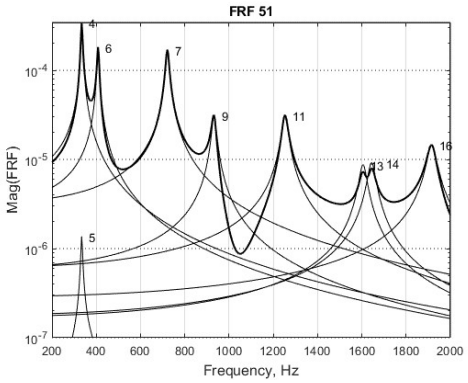

Fig. 6. Plot of FRF51.

Because the degenerated "*sine*" modes have a node in the driving point, or a very small amplitude level due to damping coupling, they cannot be excited (or weakly excited) by a single stationary harmonic force. The usual approach is to fix the rotating vectors by adding a very small mass at a reference point, e.g. at station 1.
The function $FRF11$ is presented in Fig.3 showing individual mode contributions. Because the antisymmetric "*sine"* modes 5, 8, 10, 12 and 15 have a node at $j = 1$, they are not excited by a force applied at 1, and do not contribute to the total response. It is obvious that such a plot cannot reveal double modes.
All *point* FRFs are identical, $H_{11}(\omega) = H_{22}(\omega) =.. \ . \ . \ . = H_{NN}(\omega)$. This is shown in Fig.4 where the total $FRF22$ curve, calculated as the sum of 14 individual curves of the "fixed" modes from Table 2, is identical to the total FRF11 curve.
The *transfer* FRFs calculated for different pairs of excitation and response points with the same circumferential spacing are identical. In the plots of $FRF62$ (Fig.5) and $FRF51$ (Fig.6), the total FRF curves are identical, though they are summations of different individual terms.

5. Pivoted QLP decomposition of FRF matrices

The FRF matrix $[H(\omega)]_{N_o \times N_i}$ can be calculated at N_f frequencies, for N_i excitation points and N_o response points.
The algorithm of the *pivoted QLP decomposition* [3] consists of two applications of the *pivoted QR factorization*, first to the matrix $[H]$

$$[H][\Pi_R] = [Q][R]\,, \tag{3}$$

then to the conjugate transpose of the upper triangular matrix $[R] = [Q]^H[H]\,[\Pi_R]$

$$[R]^H\,[\Pi_L] = [P]\,[L]^H. \tag{4}$$

Matrices $[Q]$ and $[P]$ have orthonormal columns and $[L]$ is lower triangular (hence $[L]^H$ is upper triangular). The pivots $[\Pi_R]$ and $[\Pi_L]$ are permutations to order the

diagonal elements of $[R]$ and $[L]^H$, respectively, in the descending order of their absolute value.

Substituting $[R] = [\Pi_L]\,[L]\,[P]^H$ into $[H] = [Q]\,[R]\,[\Pi_R]^H$, one obtains

$$[H] = \left[\hat{Q}\right]\,[L]\,\left[\hat{P}\right]^H, \tag{5}$$

where

$$\left[\hat{Q}\right] = [Q]\,[\Pi_L]\,, \quad \left[\hat{P}\right] = [\Pi_R]\,[P]\,. \tag{6}$$

This is a pivoted orthogonal triangularization of $[H]$, of the form

$$[H(\omega)] = (\text{orthogonal}) \times (\text{lower triangular}) \times (\text{orthogonal}),$$

which is cheaper than an orthogonal diagonalization like the SVD (Singular Value Decomposition) [3].

5.1. The *L*-Values Mode Indicator Function (LMIF)

The diagonal entries ℓ_{jj} of $[L]$ are called *L-values*. The LMIF is the plot of the *L*-values of the FRF matrix $[H(\omega)]_{N_o \times N_i}$ on a log-magnitude scale as a function of frequency. They track the singular values with remarkable fidelity.

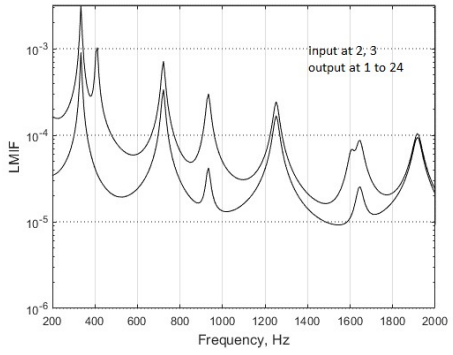

Fig. 7. LMIF plot, 24 stations.

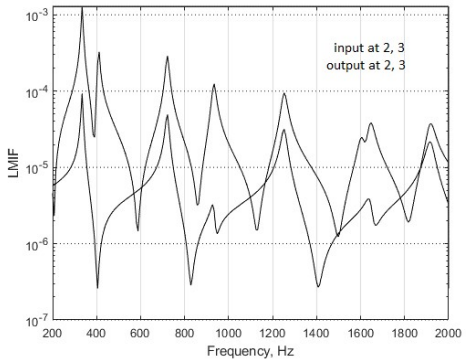

Fig. 8. LMIF plot, 2 stations.

The number of LMIF curves is equal to N_i $(N_i \leq N_o)$. The frequencies of the peaks detected in the LMIF plot give estimates for the damped natural frequencies with an accuracy which depends on the frequency resolution. The number of curves in the LMIF plot should be at least equal to the multiplicity of multiple modes.

Figure 7 shows the LMIF plot for the circular disc, for excitation in 2 and 3, and response in all 24 edge stations, with N_f =128 in the range 200 to 2000 Hz. The primary LMIF locates 8 modes and the secondary LMIF locates other 6 modes.

Figures 8 to 10 show tracked LMIF plots calculated using only two excitation and response points, hence only three FRFs each. The ability of LMIF in locating double modes is remarkable.

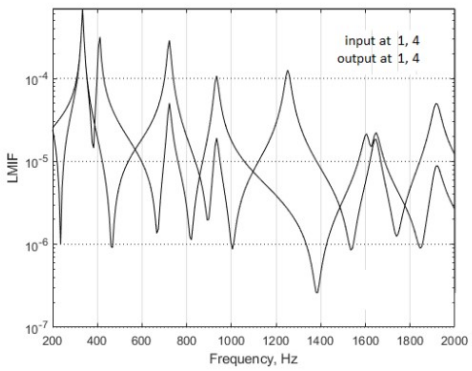

Fig. 9. LMIF plot for stations 1, 4

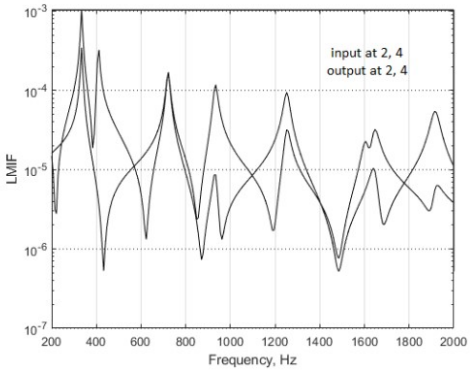

Fig. 10. LMIF plot for stations 2, 4

5.2. Analysis of QeFRF curves

The orthonormal columns of $[Q]$, referred to as *Q-vectors*, are particular linear combinations of the columns of the FRF matrix

$$\{q\}_k = \sum_{j=1}^{k} s_{jk} \{H\}_j \tag{7}$$

where s_{jk} are complex valued elements of the upper triangular matrix $[S] = [R]^{-1}$. They are used to generate an enhanced FRF with appropriate scaling.

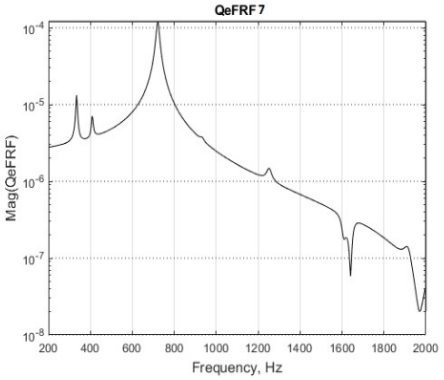

Fig.11, a. Plot of QeFRF7.

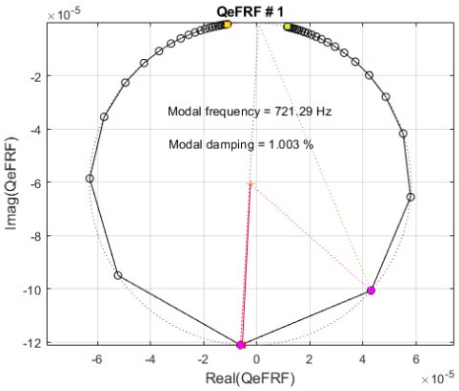

Fig.11, b. Nyquist plot of QeFRF7.

Let $\{\hat{q}\}_r$ and $\{\hat{p}\}_r$ be the columns of matrices $[\hat{Q}]$ and $[\hat{P}]$ evaluated at the *r*-th peak in the LMIF plot. They are used as spatial filters to produce a *Q-enhanced FRF* (QeFRF) for each mode of vibration

$$\{QeFRF(\omega)\}_r = SF_r \{\hat{q}\}_r^H [H(\omega)] \{\hat{p}\}_r \tag{8}$$

where the scale factor

$$SF_r = \begin{Bmatrix} \hat{p}_r(1) \\ \hat{p}_r(2) \end{Bmatrix}^+ \cdot \begin{Bmatrix} \hat{q}_r(1) \\ \hat{q}_r(2) \end{Bmatrix} \tag{9}$$

corrects the magnitude and phase of the QeFRF for the *r*-th mode. In (9) the superscript $^+$ denotes the pseudoinverse, while 1 and 2 are the locations of the (two)

driving points. The effect of this operation is to diminish the contribution of the off-resonant modes in the QeFRF [4].
Figure 11a shows the QeFRF for mode 7 calculated with N_f=521. It has a dominant peak at 721.29 Hz. The analysis of the Nyquist plot around this frequency (Fig.11b) is used to determine the modal frequency and modal damping. Good estimates of the mode shapes are obtained from the vectors $\{\hat{q}\ (\omega_r)\}_r$.

6. Pivoted QR and QLP decompositions of compound FRF matrices

Consider a Compound FRF (CFRF) matrix $[A]$ of the form

$$[A]_{N_f \times N_o N_i} = \left[\{H_{11}\}_{N_f \times 1} \quad \{H_{21}\}_{N_f \times 1} \quad \cdots \quad \{H_{jk}\}_{N_f \times 1} \quad \cdots \quad \{H_{N_o N_i}\}_{N_f \times 1}\right], \tag{10}$$

where N_i is the number of input points and N_o is the number of output points.
Each column contains the N_f frequency-dependent complex valued elements of an individual FRF, calculated at a given output/input coordinate combination.

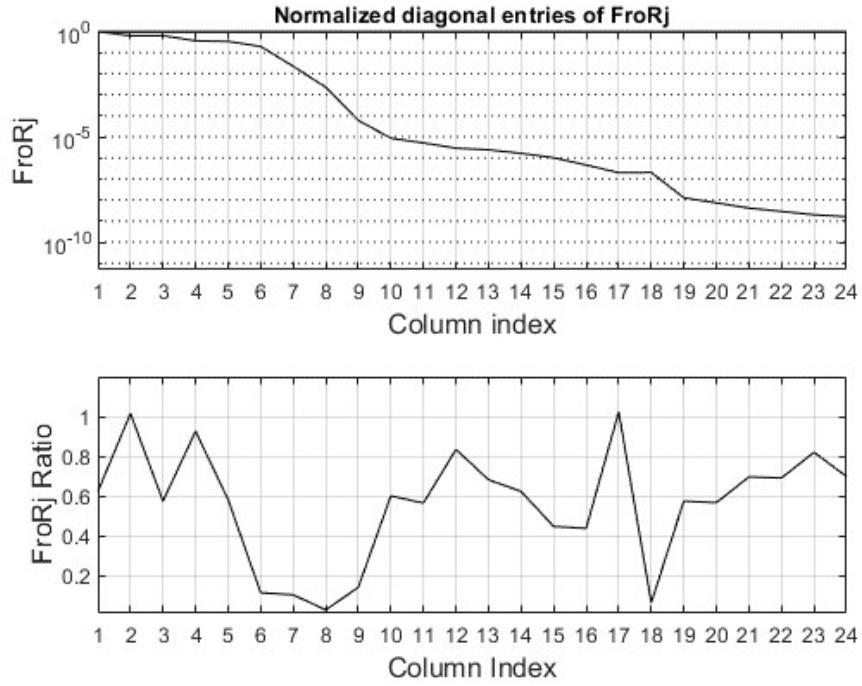

Fig. 12. FroRj plots of the axisymmetric disc.

6.1. The FroRj plots

It is possible to calculate a unitary matrix $[Q]$ and a permutation matrix $[\Pi_R]$ so that the matrix $[R] = [Q]^H [A] [\Pi_R]$ is upper triangular, hence

$$[A][\Pi_R] = [Q][R] \,, \tag{11}$$

where the same notation is maintained as before for the sake of clarity. The diagonal entries of $[R]$ are arranged in the descending order of their absolute value. They are the largest entries of each row.

Let denote by *FroRj* the magnitude values of the Frobenius norm of the rows of $[R]$. The graph of *FroRj* values versus their index (Fig.12) can be used for detecting the rank of $[A]$. A distinct through in the graph of the ratio of successive *FroRj* values indicates the numerical rank of FRF data.

The plots shown in Fig.12 and the next figures are computed using noise free FRFs for excitation at points 2 and 3, and response at all 24 edge points, for N_f =128 in the range 200 to 2000 Hz. They reveal 8 dominant modes and other 10 less prominent modes, including the contribution of off-band modes.

The diagonal entries of $[R]$ are not entirely reliable for rank detection.

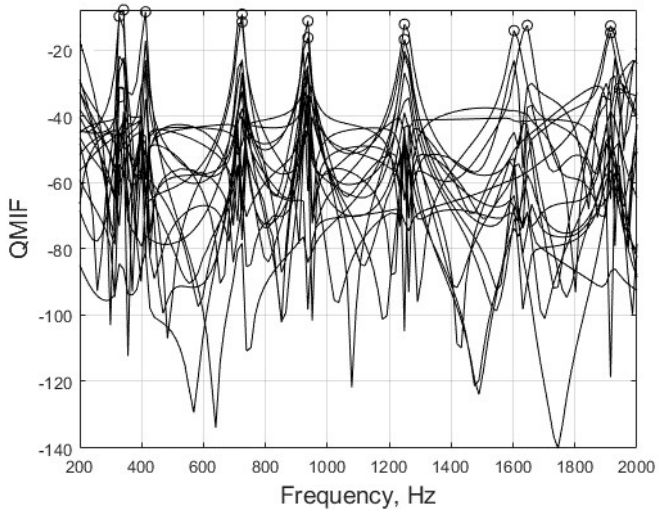

Fig. 13. QMIF plot for excitation in 2 and 3, response in 1-24.

6.2. The QMIF

The columns of $[Q]$, referred to as *Q-Response Functions (QRFs)*, are linear combinations of the original FRFs that form the columns of the CFRF matrix. They are pairwise orthogonal, hence linearly independent. Their plot versus frequency is the *Q-Vector Mode Indicator Function* (QMIF), defined as

$$\{QMIF\}_i = diag\left(\{q\}_i \{q\}_i^H\right). \tag{12}$$

The QMIF has peaks at the damped natural frequencies. It helps to estimate the number of modes active in a given frequency band but gives no indication of the

contribution of each mode to the total response. The QMIF plot presented in Fig.13 is calculated for the same numerical data as above.

6.3. The QCoMIF

The QRF Componentwise Mode Indicator Function (QCoMIF) is defined [5] by vectors of the form:

$$\{QCoMIF\}_i = diag\left(\left[I_{N_f}\right] - \{q\}_i \{q\}_i^H\right) \tag{13}$$

where $\left[I_{N_f}\right]$ is the identity matrix of order N_f.

It can be computed as the difference between a column vector of ones and the Hadamard product of the *Q*-vectors

$$\{QCoMIF\}_i = \{1\} - \{q\}_i \Theta \{q\}_i^*. \tag{14}$$

In equation (14) the star superscript denotes the complex conjugate and Θ denotes element-wise vector product.

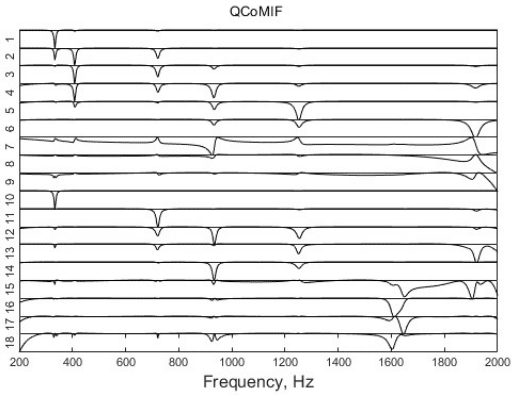

Fig. 14. QCoMIF plot for excitation in 2 and 3, response in 1-24.

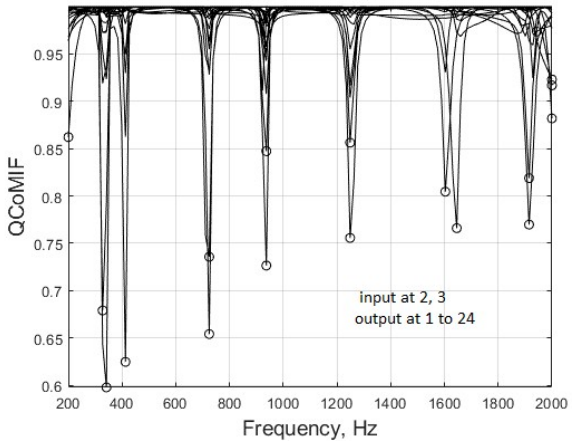

Fig.15. Overlay QCoMIF plot for excitation in 2 and 3, response in 1-24.

In the QCoMIF shown in Fig.14, the number of individual subplots is equal to 18, the estimated effective rank of the CFRF matrix. Each curve has local minima at the damped natural frequencies, with the deepest trough at the natural frequency of the corresponding dominant mode. This particular trough must be selected for each individual plot. In the selected frequency range, the plot locates 14 modes of vibration. It shows the existence of double modes even for the low frequency resolution used in this simulation. Curves 8, 9, 15, 17 account for off-range modes.
The analysis of QCoMIF requires some expertize to eliminate the information pertaining to the off-range modes. A repeated analysis in several narrower frequency bands is recommended.
An overlay of the QCoMIF curves is presented in Fig.15 for the same input/output conditions as the plot in Fig.14. The lowest trough of each curve is marked by a circle. It clearly locates the double modes and reveals the contribution of the off-range modes.

6.4. Plots of *L*-values

In the *pivoted QLP decomposition* of the CFRF matrix, the pivoted QR decomposition (11) of the matrix $[A]$ is followed by the pivoted QR factorization of the conjugate transpose of the upper triangular matrix $[R]$

$$[R]^H [\Pi_L] = [P] [L]^H. \tag{15}$$

The result is

$$[A] = [\hat{Q}] [L] [\hat{P}]^H, \tag{16}$$

where

$$[\hat{Q}] = [Q] [\Pi_L] \quad \text{and} \quad [\hat{P}] = [\Pi_R] [P]. \tag{17}$$

The pivoted orthogonal triangularization (16) provides an alternative parsimonious description of the frequency response data, being less expensive and more straightforward than the singular value decomposition [3].
The *L-values* are defined as the diagonal *elem*ents ℓ_{jj} of $[L]$. Plotting the ratio of the magnitudes of successive *L*-values, the rank of $[L]$, hence of $[A]$, is set to the index of the diagonal entry for which the ratio is a minimum [6].
The lower plot in Fig.16 shows a first minimum at index 8 and a second minimum at 18, like the *FroRj* graphs from Fig.12. It is cautious to take N_r =18 as the effective rank of $[A]$. There are 8 dominant modes, six "*cos*" modes and two modes with nodal circles, other 6 less prominent "*sine*" modes and 4 off-range modes.

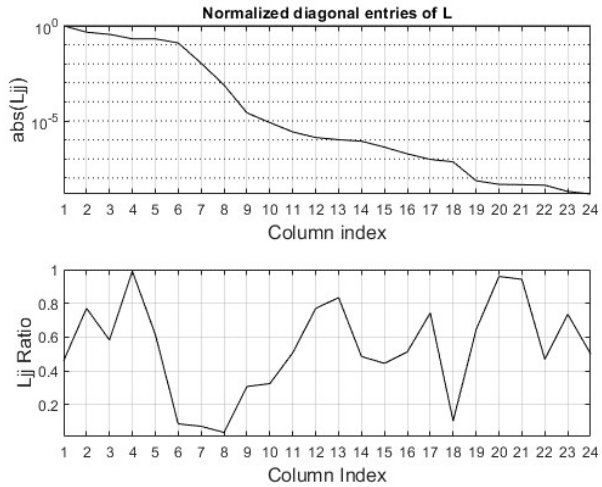

Fig.16. Plots of the L-values of the CFRF matrix, excitation in 2 and 3, response in 1-24.

7. SVD of the CFRF matrix

The Singular Value Decomposition (SVD) of the CFRF matrix can be written

$$[A] = [U]\,[\Sigma]\,[V]^H = \sum_{i=1}^{N} \sigma_i \{u\}_i \{v\}_i^H = \sum_{i=1}^{N} [A]_i, \qquad (18)$$

where $\{U\}$ and $\{V\}$ are the matrices of the left and right singular vectors, respectively. The singular values σ_i are arranged in non-increasing order of magnitude in the real diagonal matrix $[\Sigma]$.

The upper part of Fig.17 is a plot of magnitudes of the singular values versus their index, normalized to the largest one. The lower graph shows the ratio of successive singular values. The graphs resemble those from Figs. 12 and 16. The *L*-values track the singular values remarkably well.

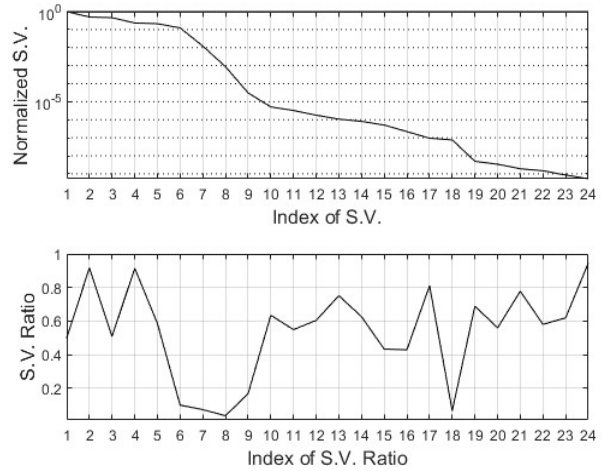

Fig. 17. Plots of the singular values of the CFRF matrix, excitation in 2 and 3, response in 1-24.

7.1. The UMIF

The left singular vectors contain the frequency distribution of the energy, being linear combinations of the original FRFs that form the columns of $[A]$. Their plot versus frequency is the *U-Vector Mode Indicator Function* (UMIF) [7]. The UMIF has peaks at the damped natural frequencies.

The UMIF shown in Fig.18 is similar to the QMIF plot from Fig.13, exhibiting peaks at the damped natural frequencies.

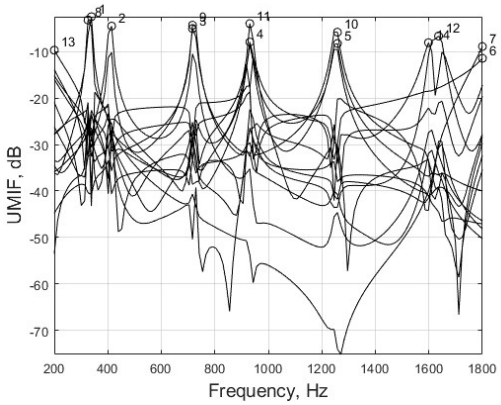

Fig. 18. UMIF of circular disc.

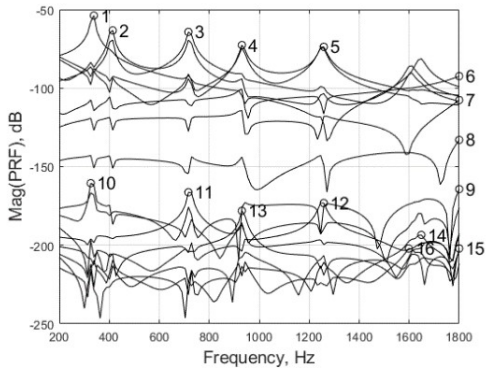

Fig. 19. Plot of PRFs

7.2. Principal Response Functions (PRFs)

The Principal Response Functions, $\{p\}_i$, defined as the left singular vectors scaled by the respective singular values, are linear combinations of the original FRFs, $\{a\}_j$:

$$\{p\}_i = \sigma_i\{u\}_i = [A]\{v\}_i = \sum_{j=1}^{N} v_{ji}\{a\}_j. \tag{19}$$

The PRF plot from Fig.19 is calculated for the same input/output conditions as the UMIF plot in Fig.18. The important modes are clearly separated in the upper part of the graph from the modes with low energy revealed by peaks in the lower curves.

7.3. The Componentwise Mode Indicator Function (CoMIF)

The Componentwise Mode Indicator Function is defined [8] by vectors

$$\{CoMIF\}_i = \{1\} - \{u\}_i \odot \{u\}_i^*. \qquad (20)$$

computed as the difference between a column vector of ones and the Hadamard product of the left singular vectors. In equation (32) the star superscript denotes the complex conjugate.

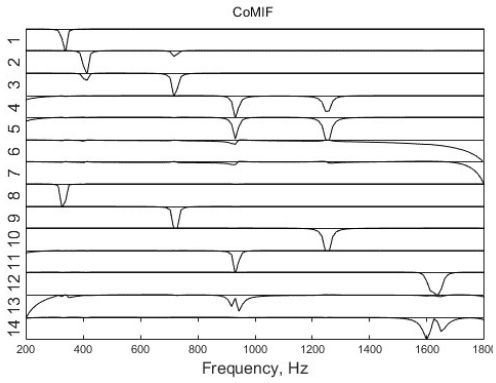

Fig. 20. CoMIF with subplots.

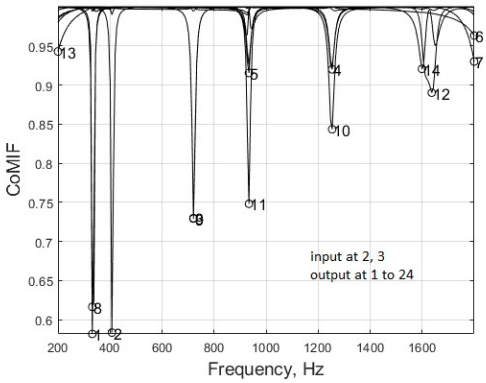

Fig. 21. CoMIF with overlaid curves.

The CoMIF plot with individual curves displayed separately in subplots is shown in Fig. 20. The CoMIF plot with overlaid curves is shown in Fig.21. Both CoMIF plots clearly locate all modes of vibration in the selected frequency range and reveal the existence of double modes.

8. Concluding remarks

This paper has presented an alternative way of modal analysis based on the QLP decomposition with column pivoting of a collection of FRFs. It closely parallels and extends the previously developed techniques based on the SVD of FRF matrices.

Several Mode Indicator Functions have been developed and their performance was assessed using simulated numerical FRF data for a lightly damped circular disc. For the low modal damping value introduced to obtain realistic FRFs, the mode complexity is low and the complex mode results are nearly the same as for the real modes.

The *L*-values are related to energy. Their plot versus frequency, referred to as the LMIF, has been found to be very efficient to assess the proper number of modal frequencies, even for a small number of excitation/response stations and noisy data. The LMIF agrees with the CMIF as the *L*-values tend to track the singular values of FRF matrices.
The effective rank of CFRF matrices, hence the number of active modes present in a frequency range, is well estimated using plots of *L*-values versus their index and FroRj graphs, which are similar to the singular value plots.
Modal parameters can be determined using enhanced QeFRFs and a circle-fit single-degree-of-freedom parameter identification technique. The *Q*-vectors estimated at the frequencies of the peaks in the LMIF graph are approximate eigenvectors. The quality of the approximation depends on the relative amplitude of the response in the resonant mode with respect to the responses of the non-resonating modes.
The QCoMIF based on the *Q*-vectors of the reordered CFRF matrix is similar to the CoMIF based on the left singular vectors.
All presented mode indicators can reveal double modes of lightly damped structures.

References

[1] Thomas D.L., *Dynamics of Rotationally Periodic Structures*, Int. J. for Numerical Methods in Engineering, **14**, 1979, p. 81-102.
[2] Ewins D.J., *Modal Testing: Theory, Practice and Application,* 2nd ed., Research Studies Press, Baldock, U.K., 2000.
[3] Stewart G.W., *Matrix Algoritms, vol.1: Basic Decompositions*, SIAM, Philadelphia, 1998.
[4] Phillips A.W., Allemang R.J., Fladung W.A., *The Complex Mode Indicator Function (CMIF) as a Parameter Estimation Method,* Proc.Int. Modal Analysis Conf. IMAC-16, Santa Barbara, CA, 1998, p. 705-710.
[5] Radeş M., Ewins D.J., *MIFs and MACs in Modal Testing,* Proceedings of IMAC-20 Conference on Structural Dynamics, Los Angeles, CA, 2002, p. 771-778.
[6] Radeş M., Ewins D.J., *Analysys of FRF Test Data Using the Pivoted QLP Decomposition*, Proc. Int. Conf. "Structural Dynamics Modeling – Test, Analysis, Correlation and Validation", Madeira, Portugal, 2002, p. 509-516.
[7] Radeş M., *Condensation of Frequency Response Test Data by the QR Decomposition,* Proc.Int. Conf. "Noise and Vibration Engineering", Leuven, Belgium, 2000, p. 1241-1246.